Manumula Srinubabu[1*]
Praveen Nagadasu[2]
Mohiddin Shaik[2]
A. Kondababu[3]

Design and Analysis of a 4-Element Compact MIMO Antenna for 5G n78/n79/n48 Band Communication

Journal of Electrical Systems

Abstract: - This paper presents an irregular polygon design with a unique protruding strip that has been specifically developed for 5G NR n78/n79/n48 applications, resulting in a compact and efficient 4-element MIMO antenna. The antenna measures 31.25 × 41.25 × 1.6 mm³, utilizing an FR-4 substrate with a ε_r of 4.4. It achieves a wide impedance bandwidth ($S_{xx} < -10$ dB) covering the 3.15–3.89 GHz frequency range. The structure includes a 2-element MIMO antenna with elements spaced just 0.012 λ0 apart, paired with another orthogonally arranged 2-element MIMO antenna. The design employs a microstrip feeding line with a partially truncated ground, complemented by embedded grounded stubs to enhance isolation. Additionally, T- and I-shaped decoupling elements positioned between the radiators further extend the bandwidth and improve isolation (S_{xy}) across the band. Despite its compact size, the antenna effectively reduces coupling, achieving isolation levels (S_{xy}) better than −18.25 dB throughout the operating range. It delivers a peak gain of 3.79 dBi and boasts an excellent radiation efficiency of 86%–92%. The MIMO performance is characterized by a total active reflection coefficient (TARC) of −10 dB, a mean effective gain (MEG) of 1 dB, and a channel capacity loss (CCL) of below 0.175 bits/s/Hz. The antenna also demonstrates an outstanding envelope correlation coefficient (ECC) of 0.028 and a diversity gain (DG) of 9.9 dB, making it highly suitable for 5G NR n78/n79/n48 communication applications.

Keywords: MIMO Antenna, Protruding strips, Truncation Ground, Defected ground structure (DGS), Decoupling Elements (DE), Diversity Parameters, Sub-6 GHz Communication.

I. INTRODUCTION

In today's world, enhancing the capacity, data rate, and bandwidth of 5G communication and maintain low latency, as outlined by the Third-Generation Partnership Project (3GPP) [1,2]. MIMO technology has been identified as a key solution in 5G specifications for addressing these demands [3–5]. By leveraging MIMO, wireless systems achieve improved throughput and diversity performance through enhancements in parameters such as isolation, envelope correlation coefficient (ECC), diversity gain (DG), total active reflection coefficient (TARC), and channel capacity. However, the performance of MIMO systems can be compromised by interference arising from the close placement of antenna elements. To overcome this challenge, various isolation techniques have been developed [6–8], including element decoupling methods [9–11], the use of neutralization lines [12], stubs [13–16], defective ground structures (DGS) [17–19], polarization techniques [20], electromagnetic band gap (EBG) structures [15, 21, 22], and metamaterials [23, 24]. These methods work by manipulating the interaction between antennas, such as altering or suppressing surface current flow, to reduce interference and minimize signal overlap [25, 26].

MIMO antennas are typically designed with various dimensions and techniques to achieve optimal isolation and performance. For instance, some configurations, measuring 180 × 180 mm², utilize ground stubs and slots to improve isolation, as reported in [9]. A smaller metallic MIMO antenna, with dimensions of 45 × 32 mm², has demonstrated a significant 25 dB isolation enhancement, according to [27]. Another design features antenna elements spaced 5 mm apart, utilizing a mirroring technique within a 40 × 40 mm² footprint, maintaining high performance as noted in [21]. Further, antennas with element sizes of 64 × 32 mm², 65 × 35 mm², and 66.8 × 40 mm² [18, 23-24] are arranged in parallel with spacing of 8 mm and a minimal 1 mm gap, ensuring compactness and functionality. Another design, measuring 42.6 × 52 mm² [28], consists of two parallel, oppositely oriented binary antennas sharing a connected ground. This setup employs isolation branches to enhance performance, covering a bandwidth of 1.8–2.65 GHz with a 21.4 mm spacing between the antennas. In a 4×4 MIMO configuration, a monopole antenna with dimensions of 66 × 66 mm² [29] achieves isolation levels exceeding 21 dB. Notably, this design avoids using decoupling elements between the elements, preserving its compact size, with an 8 mm gap separating them. Another innovative fractal antenna design, employing CPW feeding, measures 57 × 34 mm² [30] and features an orthogonal MIMO arrangement. The inclusion of a neutralization line as a decoupling element enhances isolation (S_{21}) by an impressive 45 dB. Lastly, an antenna configuration documented in [31] with dimensions of 32 × 47 × 0.8 mm³ further exemplifies the integration of advanced techniques to achieve superior isolation and bandwidth performance. A 2-port MIMO antenna with dimensions of 63.2 × 54.2 × 0.584 mm³ operates within the 3.35–3.85 GHz frequency range, utilizing techniques such as defected ground structures (DGS) and branching T-elements. It achieves an isolation level of $S_{21} = -15.15$ dB and an efficiency of 85%, making it suitable for n78 band communication [32]. Other 4-element MIMO antenna designs include a 34 × 129.5 × 1.6 mm³ antenna [3] and a 64.5 × 78 × 1.6 mm³ antenna [33], both employing DGS and decoupling methods. These antennas cover frequency bands of 2.25–4.25 GHz, 2.21–2.25 GHz, and

[1*]VIT-AP University,Amaravati, A.P., srinubabu.21PHD7112@vitap.ac.in
[2]Asst. Prof. , ECE Dept., Sri Sarathi Institute of Engineering and Technology., nagadasupraveen@gmail.com and mohiddin9705@gmail.com
[3]Aditya University,Surampalem, Kakinada. kondababu.amaradi@adityauniversity.in
***Corresponding Author:** Manumula Srinubabu
*VIT-AP University, srinubabu.21PHD7112@vitap.ac.in

2.53–3.65 GHz, achieving isolation levels below −22 dB at their respective operating frequencies, tailored for sub-6 GHz applications. The gap between the two radiators has been reduced to just 1.5 mm (0.0174λ₀), optimizing compactness. A mirror image of the first radiator was applied to improve the S_{xy} value using mirroring techniques. The electrical length of the patch element has been extended without increasing the overall antenna dimensions, ensuring space efficiency. A truncated ground plane was incorporated, accompanied by grounding stubs and side stubs, to enhance both bandwidth and isolation (S_{xy}). Protruded strips were added to the patch to support higher frequency bands while maintaining excellent isolation. Additionally, a T and I-stubs has been strategically placed between the radiators to significantly improve isolation. These combined methods contribute to the innovative features of the design, offering a compact footprint and superior isolation. To address the growing demands in modern communication systems, this research presents a novel antenna design that achieves these objectives effectively. This paper is organized as follows: the first section covers the antenna design and methodology, followed by the presentation and analysis of results, and concludes with a summary of the findings.

II. ANTENNA DESIGN AND METHODOLOGY

The design process begins with an irregular pentagonal monopole antenna featuring a protruded strip and a truncated ground embedded with grounding stubs. This initial design was expanded into a 2-element MIMO antenna measuring 20 × 31.5 × 1.6 mm³, with the intra-element gap minimized to enhance isolation. The configuration was further developed into a 4-element MIMO antenna by arranging two 2-element MIMO antennas orthogonally. This compact 4-element design has dimensions of 31.25 × 41.25 × 1.6 mm³ and is tailored for sub-6 GHz communication. The antenna is designed on an FR-4 substrate with an ε_r of 4.4 and a loss tangent of 0.002.

A. Single Monopole Antenna Design

The design process commenced with Ant.1, a pentagonal patch antenna featuring a partial ground plane, as illustrated in Fig. 1(b). However, it failed to meet the desired frequency band coverage requirements. To overcome this limitation, Ant.2 was developed, incorporating a circular patch with radius R and a modified ground plane with an elliptical cut, characterized by parameters g and h. While Ant.2 achieved resonance at a higher frequency band, further refinement was necessary to enhance its performance.

Ant.3 introduced improvements by integrating microstrip feeding elements (l_5=2.56 mm, l_6=2.88 mm) and an irregular patch design, leading to an improved bandwidth compared to Ant.2. The goal was to create a compact, electrically efficient antenna capable of operating across the 3.3–3.8 GHz band, suitable for N78/48/79 band communication. Building on these advancements, Ant.4 employed slit optimizations with dimensions l1=1.9 mm, l_2=4.8 mm, l_3=2.88 mm, and W_1=1 mm. Additional slit dimensions l_4=4.8 mm, l_7=6.73 mm, and W_1 were introduced to further extend the electrical length and optimize bandwidth. Ant.5 implemented a protruded strip in the radiator design, achieving superior bandwidth centered at 3.5 GHz. The protruded strip was carefully optimized with dimensions p_1=2.2 mm and p_2=5.9 mm, enabling broader bandwidth and shifting the operating frequencies to lower values. The progression and characteristics of these designs are presented in Fig. 1(b). This stage also featured a modified ground plane and additional protruded strips, ensuring symmetric and stable electromagnetic behavior, thereby enhancing radiation characteristics and overall performance. The final optimized monopole antenna designs are depicted in Fig. 1(a). The antenna is fed through a microstrip insert feed line with dimensions $L_f \times W_f$=8.45×1.85 mm², offering a 50 Ω impedance and excited using a lumped port.

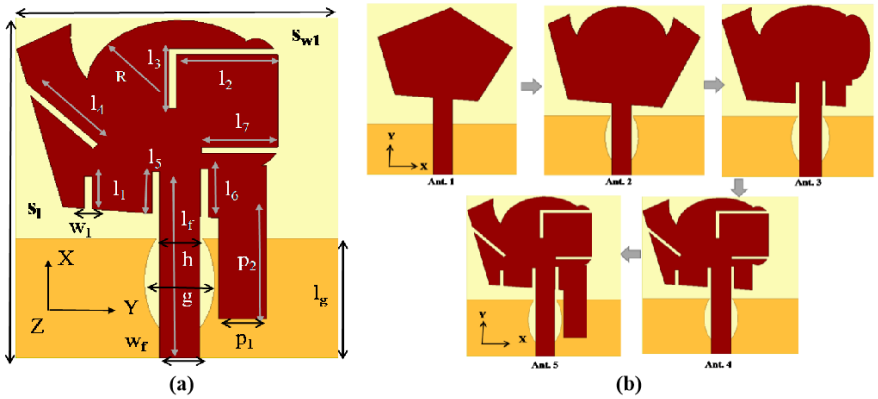

Fig. 1. (a) Optimized single monopole antenna with dimensions. (b) Iterative evolution of the monopole antenna from Ant.1 to Ant.5.

B. 2-Element MIMO Antenna Design

The 2-element antenna design consists of two polygonal radiators with circular elements, connected by extended strips, and incorporates a T-shaped stub between the elements to significantly enhance isolation. This compact prototype measures 20 × 31.5 × 1.6 mm³, with an inter-element spacing of 1.5 mm (0.012λ_0 at 3.5 , GHz) in Fig. 2(a). Figure 2(b) illustrates the iterative evolution of the 2-element MIMO antenna aimed at optimizing isolation and bandwidth for the target n77/48/79/78 band. Ant. A features symmetrical antennas with a mirrored first element to improve isolation, supported by a separate ground. To enhance the S_{21} parameter, a rectangular slot is etched into the common ground. Although S21 is improved at

3.6 GHz, the design does not cover the entire frequency band, and S_{21} remains below −12 dB in both cases. Next, Ant. C introduces an inverse T-shaped grounded vertical stub integrated into the ground plane, achieving an S_{21} below −12 dB across the full n78/48 band. The stub's dimensions, including width (a), length (b), and the bottom rectangular height (f) between the ground and stub, are set to 2.33 mm, 11.85 mm, and 1 mm, respectively. Finally, Ant. D incorporates additional side stubs alongside the ground stub, resulting in an S_{21} of less than −15.5 dB. The side stub dimensions, including width (c), length (d), and the gap between the side and grounded stubs (e), are 1.25 mm, 7 mm, and 0.9 mm, respectively.

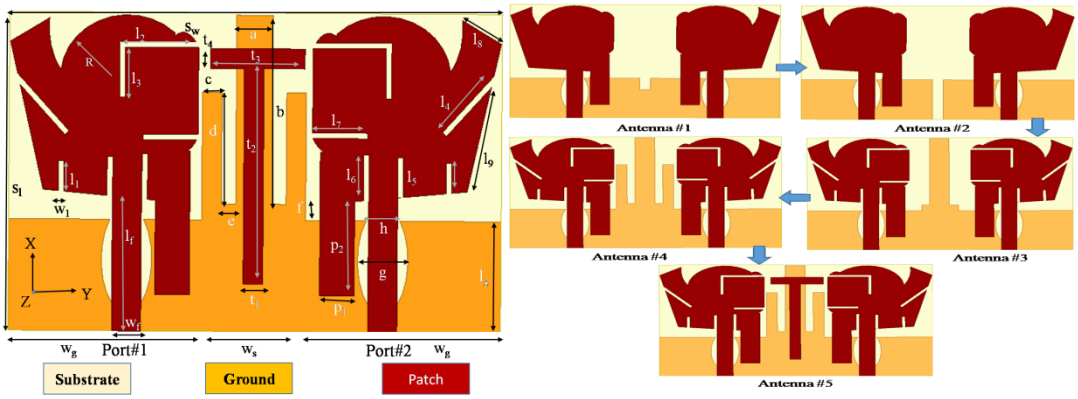

Fig. 2. (a) Optimized 2-element MIMO antenna with dimensions. (b) Evolutionary progression of the two-port MIMO antenna design.

*C. **Proposed 4-Element MIMO Antenna Design***

Figure 3 displays the front and rear views of the optimized 4-element MIMO antenna. Two 2-element MIMO antennas are arranged orthogonally to achieve spatial diversity, resulting in a compact overall size (p x q) of 31.25 × 41.25 × 1.6 mm³ with a common ground plane. The ground plane connects the rectangular elements, with each element having a width (t) of 1.45 mm and a length (s) of 3 mm. The resulting S_{xy} is below −15.5 dB. To further enhance isolation, a horizontal I-shaped element (length = 31 mm, width (r) = 0.8 mm) is integrated into the common ground, modifying the current distribution across the ground and patches, which improves the isolation to below −16.15 dB. Additionally, a I-shaped decoupling element of identical dimensions is strategically placed between the two 2-element MIMO antennas, resulting in S_{xy} levels below −18.25 dB across the full operating band. The proposed 4-element MIMO configuration achieves a more compact size at 3.5 GHz and an enhanced bandwidth of 740 MHz (3.15–3.89 GHz). The fractional bandwidth is calculated as (3.89–3.15) / 3.52 GHz = 0.8559, which corresponds to a percentage of 85.59%. The design successfully covers the desired operating band, with S_{xy} maintained below −18.25 dB. This design is well-suited for modern 5G sub-6 GHz communications.

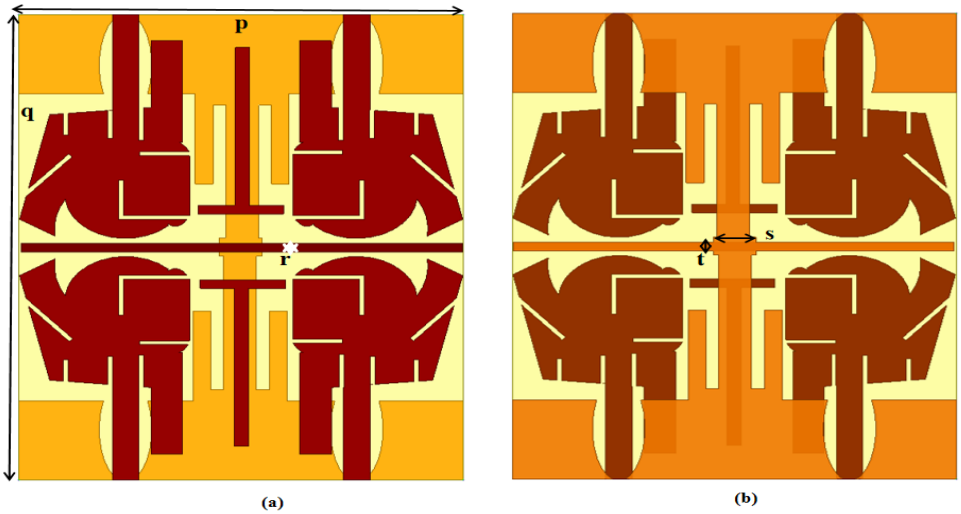

Fig. 3. Optimized 4-element MIMO antenna with dimensions. (a) Front View (b) Rear View.

Decoupling elements are strategically placed in antenna designs to reduce electric field coupling between adjacent elements. The arrangement and spacing of these elements play a critical role in this process. By carefully positioning the radiators, the electric and magnetic fields between them are altered, effectively creating a barrier that disrupts the coupling paths. This is achieved by adjusting the impedance matching, which helps minimize the coupling effects. Modifying the distance and orientation of the elements can further improve isolation. The coupling coefficient (Cc) quantifies the interaction between antennas (i and j), as expressed in equation (1) [37].

$$|C_c^2| = \frac{|S_{21}|^2}{\sqrt{(1-|S_{11}|^2)*(1-|S_{11}|^2)}} = S_{21_{mag}} * e^{j*S_{21\,phase}} \quad (1)$$

S_{21} calculating the based on simulates S-parameter values and its covers the -15 dB, the coupling coefficient $|C_c^2| = 10^{(S_{21}/20)} = 10^{(-18.25/20)} = 10^{-0.9125} \approx 0.1223$. The coupling coefficients play a crucial role in determining the isolation level between the antenna ports. The isolation (I) is computed using equation (2) [38], where the isolation due to the coupling coefficient is given by $I = -20\log_{10}(Cc)$.

$$\text{Isolation} = I = 20\log_{10}\left(\frac{1}{\sqrt{(1-|S_{21}|^2)}}\right) \quad (2)$$

$I = -20\log_{10}(0.1223) = --20(-0.9126) \approx 18.14$ dB. The isolation between the radiators is affected by the T-stub element shown in Fig. 3, which functions as a capacitance. Given that the wavelength λ=c/f=3003.5=85.71 mm, it is approximated to be 86 mm. The λ/4 = 23 mm. When the stub length exceeds 15 mm, it behaves as a capacitive impedance and effectively remains open-circuited.

*D. **Surface Current distribution (SCD)***

First, confirm that you have the correct template for your paper size. This template has been tailored for output on the US-letter paper size. If you are using A4-sized paper, please close this template and download the file for A4 paper format called "CPS_A4_format". Figure 4 presents the surface current distribution (SCD) for 2-element and 4-element MIMO antenna configurations, with and without decoupling elements. Fig. 4(a) shows the SCD of a 2-element MIMO antenna with a ground stub and two side stubs placed on the ground plane.

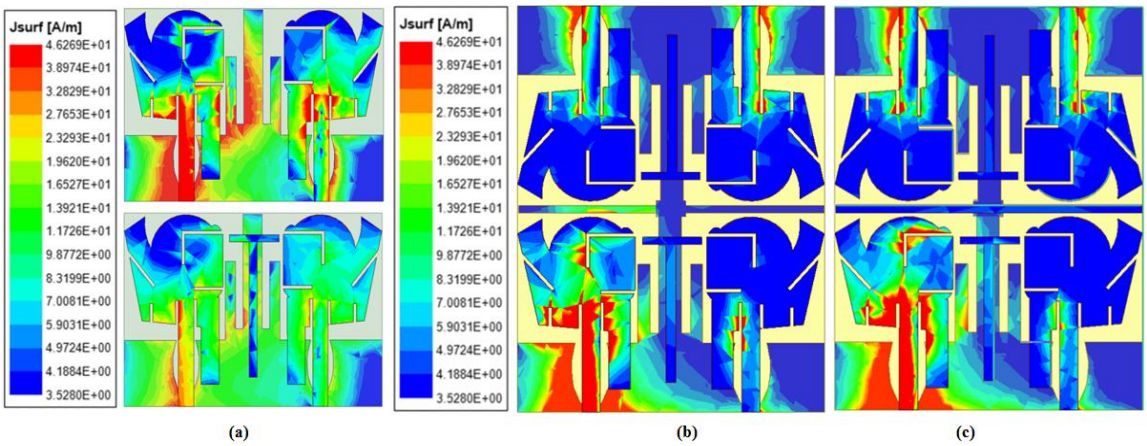

Fig. 4. Surface Current Distribution (SCD): (a) Two-element MIMO antenna with and without a T-shaped stub. (b) Four-element MIMO antenna with a common ground. (c) Proposed four-element MIMO antenna with a horizontal decoupling element.

Additionally, a protruded strip with a radiator is included, which helps limit current spreading and improves isolation. The use of a T-stub between the radiators enhances the current distribution, improving S_{21} by more than 19 dB compared to the configuration without the T-stub. Fig. 4(b) illustrates the SCD for a 4-element MIMO antenna with a common ground. While the common ground, shared by all four radiators, alters the current distribution and reduces S_{xy} compared to the 2-element design, it introduces interference due to the shared structure. Fig. 4(c) shows the proposed 4-element MIMO antenna equipped with a horizontal decoupling element. This element acts as a reflector, reducing interference and improving S_{xy} by up to 15 dB compared to the 2-element configuration. The variations in surface current distribution across these designs.

III. RESULTS AND DISCUSSION

Figure 5(a) illustrates the iterative simulation results for the single monopole antenna design. Ant. 1 exhibits a wide sub-6 GHz bandwidth centered at 3.6 GHz but shows poor impedance matching (S_{xx}). Ant. 2 improves the bandwidth, extending from 3.5 GHz to 4.1 GHz, with a center frequency of 3.79 GHz. Ant. 3 covers a range of 3.3–3.75 GHz, centered at 3.5 GHz, achieving S_{xx} of -15 dB. Ant. 4 depicts poor impedance matching, with a bandwidth below 3 GHz up to 3.85 GHz and a center frequency of 3.4 GHz. The optimized antenna (Ant. 5) achieves an impedance bandwidth of 650 MHz (3.2–3.85 GHz) with S_{xx} < -10 dB and excellent impedance matching of -35 dB at the resonance frequency.

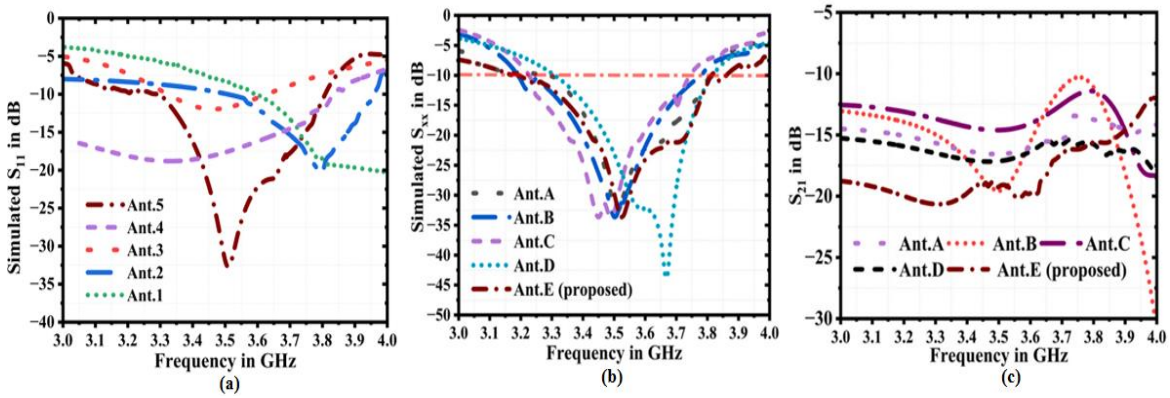

Fig. 5. (a) Simulated S_{xx} results for the single antenna design evolution and S-parameter results of the 2-element MIMO antenna design evolution (b) S_{xx} results (c) S_{xy} results.

Figure 5(b) and (c) presents the simulation S_{xx} and S_{xy} results for the step-by-step evolution of a 2-element MIMO antenna design from Ant. A to Ant. E. Ant. A achieves a wide sub-6 GHz bandwidth with excellent impedance matching (S_{xx} = -30 dB) but suffers from poor isolation (S_{21}). Ant. B shows a shift of the higher bandwidth to a lower band, resonating at 3.5 GHz, with S_{21} improving to -12 dB. Ant. C narrows the bandwidth and achieves S_{21} < -13 dB. Ant. D extends the lower band from 3.32 to 3.8 GHz, achieving S_{xx} = −45 dB at 3.69 GHz. The isolation (S_{xy}) improves, staying above 16 dB across the operating band. The optimized 2-element MIMO design, represented as Ant. E, achieves a bandwidth of 600 MHz (3.25–3.85 GHz) with enhanced isolation. The isolation parameter (S_{21}) reaches -19 dB, a significant improvement from the earlier −16 dB.

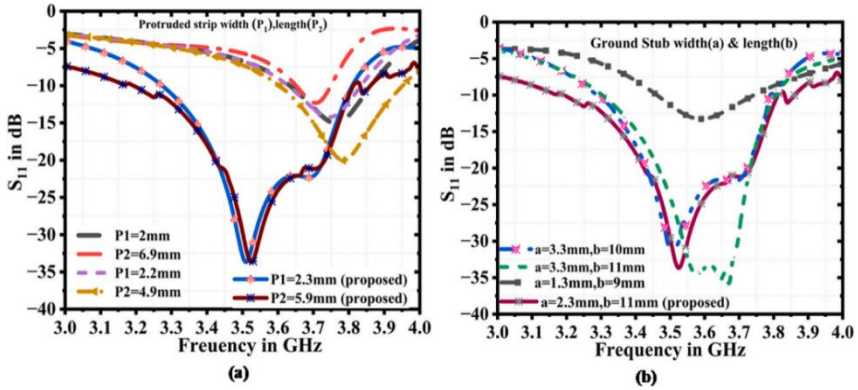

Fig. 6. Simulated results of parametric studies: (a) Protruded stub length and width variation (b) Grounded stub length and width variations

Figure 6(a) illustrates the parametric analysis and optimized dimensions of the protruded stub, denoted as P_1 and P_2, which play a crucial role in enhancing both bandwidth and isolation. The width of P_1 can be adjusted between 2.2 mm and 2.4 mm, with 2.3 mm identified as the optimal value. Similarly, P_2 can vary between 4.9 mm and 6.9 mm, with 5.9 mm being the optimal dimension. Effective isolation is achieved for two closely spaced antenna elements with a separation of 1.5 mm (w_s), ensuring compliance with the bandwidth requirements for the N78/48/79/77 bands at 3.5 GHz. Figure 6(b) highlights the optimal dimensions for the width (a) and length (b) of the ground stub, which significantly influence bandwidth performance. The width (a) is adjustable from 1.3 mm to 3.3 mm, with 2.3 mm being the most effective. The length (b) ranges from 9 mm to 11 mm, with optimal performance achieved at 11 mm. These refined dimensions enable the antenna to meet the required bandwidth specifications, achieving an S_{21} isolation of −35 dB at 3.5 GHz.

Figure 7(a) shows the impact of varying the partial ground length (lg), where increasing the length from 6.5 mm to 7.5 mm results in a decrease in the frequency band from higher to lower frequencies, with the optimal length being 7 mm. For the T-stub, the length (t2) is optimized at 15 mm, and the width (t1, t4) ranges from 1 mm to 1.5 mm, with the best performance achieved at 1.25 mm. At these optimized values, the antenna covers the N78/48 band (3.25–3.85 GHz), and the isolation (S21) improves from 16 dB to 19.25 dB across the entire band. For other dimensions, isolation is covered in 70–80% of the band. In Fig. 7(b), the isolation is increasing from 13 dB to 16 dB. The inclusion of decoupling elements in the antenna design plays a crucial role in minimizing electric field coupling between adjacent elements. The simulated S_{xx} results of the proposed 4-element MIMO antenna are presented in Fig. 8. The antenna achieves an impedance bandwidth (S_{xx} <−10 dB) of 740 MHz, spanning from 3.15 GHz to 3.85 GHz, with a resonance frequency of 3.5 GHz.

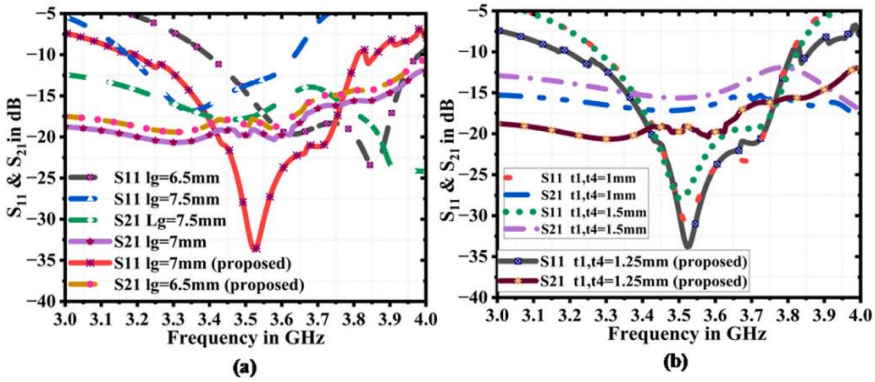

Fig. 7. Simulated results of parametric studies: (a) Partial ground length variation (b) T-shaped stub with different widths

This represents an enhancement in bandwidth compared to the 2-element MIMO antenna. The impedance matching is significantly improved, reaching −39.5 dB, making the design highly suitable for modern sub-6 GHz band communication systems.

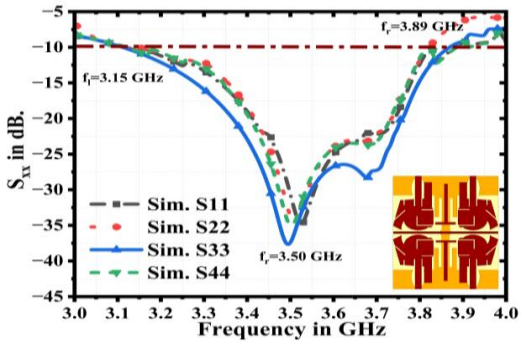

Fig. 8. Simulated S_{xx} results of the proposed 4-element MIMO antenna

Figure 9 illustrates the simulated S_{xy} results for different configurations, with and without the I-shaped decoupling element (ISDE). The ISDE is strategically positioned between the two 2-element MIMO antennas, playing a critical role in improving the S_{xy} values across the operating band of the proposed 4-element MIMO antenna. Figure 9(a) shows the parametric analysis of S_{xy} results based on the ISDE width (r), which varies between 0.7 mm and 1 mm. The optimal width is found to be 0.8 mm, achieving S_{xy} below −18.25 dB across the entire operating band. Figure 9(b) compares the S_{xy} results with and without the ISDE. The inclusion of the ISDE improves S_{xy} from −16.50 dB to −18.25 dB, resulting in a -1.75 dB enhancement. This optimization significantly enhances the performance of the 4-element MIMO antenna.

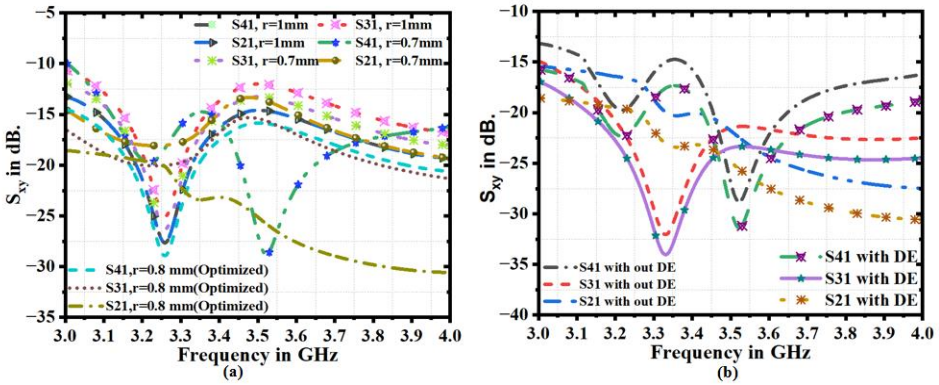

Fig. 9. Simulated S_{xy} results of the proposed 4-element MIMO antenna (a) Parametric of I-shaped decoupling element (ISDE) width (r) and (b) with and with out I-shaped decoupling-element(ISDE)

The diversity performance significantly influences the configuration of MIMO antennas. Key metrics such as envelope correlation coefficient (ECC), diversity gain (DG), total active reflection coefficient (TARC), mean effective gain (MEG), and channel capacity loss (CCL) are used to evaluate performance. For optimal MIMO antenna operation, the coupling between individual radiating elements must be minimal. The ECC, which depends on factors like the radiation pattern, polarization, and relative phase of the fields, can be calculated using the equation 3 [3, 5]. Ideally, ECC values should approach 0.5 or lower. The simulated ECC for the proposed design ranges from 0.001 to 0.45 across the operating frequency band, as shown in Fig. 10(a).

$$ECC = |\rho_e(i,j,N)| = \frac{\Sigma_{n=1}^{N} S_{i,n}^{*} S_{n,j}}{\Pi_{k(=i,j)}\left[\Sigma_{n=1}^{N} S_{i,n}^{*} S_{n,k}\right]} \quad (3)$$

Here, i, j, N =1 to 2 (for two elements)

$$D.G. = 10\sqrt{1-\rho_e{}^2} \quad (4)$$

High interaction between antenna components can reduce diversity gain (DG), which is derived from ECC using the formula in 4 [3, 5]. Ideally, DG should be around 10 dB. Simulation results for the MIMO antenna indicate DG values ranging from 9.7 to 9.99 dB, also illustrated in Fig. 10(a). Equation (5) [3, 5, 26, 41, 42] is used to calculate the TARC, which typically falls within the range of 0 to 1. The reflection coefficient S_{11} starts at -10 dB, defining the bandwidth, and reaches -26 dB at the resonance frequency, as depicted in Fig. 10(b).

$$TARC = \Gamma = \frac{\sqrt{\left((S_{11}+S_{12}e^{j\theta})^2+(S_{21}+S_{22}e^{j\theta})^2\right)}}{\sqrt{4}} \quad (5)$$

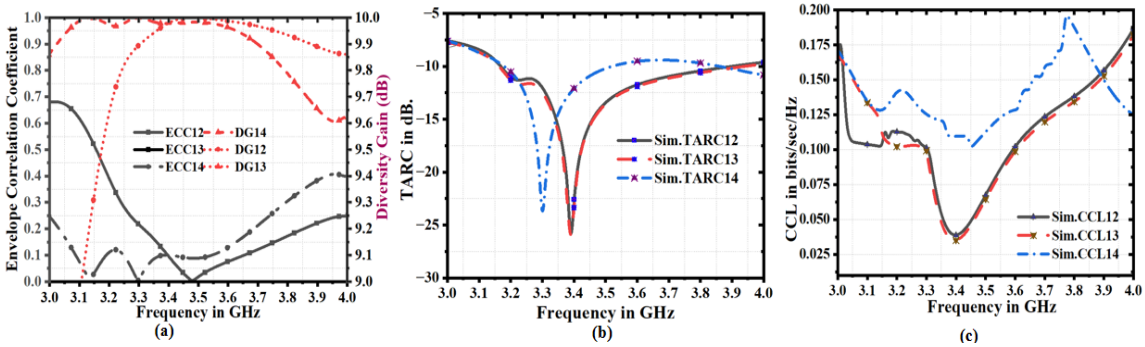

Fig. 10. Simulated results of the proposed 4-element MIMO antenna (a) ECC and DG (b) TARC (c) CCL

The channel capacity loss for the two elements is calculated using Equation (6) [3, 33], with the simulated results shown in Fig. 10(c). Across the N78/48 band, the channel capacity loss ranges from 0.012 to 0.13016 bps/Hz, with a minimum loss of 0.0107 bps/Hz occurring at the resonance frequency of 3.45 GHz.

$$CCL_{ij} = -log_2(\varphi^{\epsilon}), \quad (6)$$

$$here\ \varphi^{\epsilon} = \begin{bmatrix} \omega_{ii} & \omega_{ij} \\ \omega_{ji} & \omega_{jj} \end{bmatrix},$$

$$w_{ii} = 1-\left(|S_{ii}|^2+|S_{ji}|^2\right), \omega_{ij} = -\left(S_{ii}^{*}S_{ij}+S_{ji}^{*}S_{jj}\right),\ \omega_{ji} = -\left(S_{jj}^{*}S_{ji}+S_{ij}^{*}S_{ii}\right); \omega_{jj} = 1-\left(|S_{jj}|^2+|S_{ji}|^2\right)$$

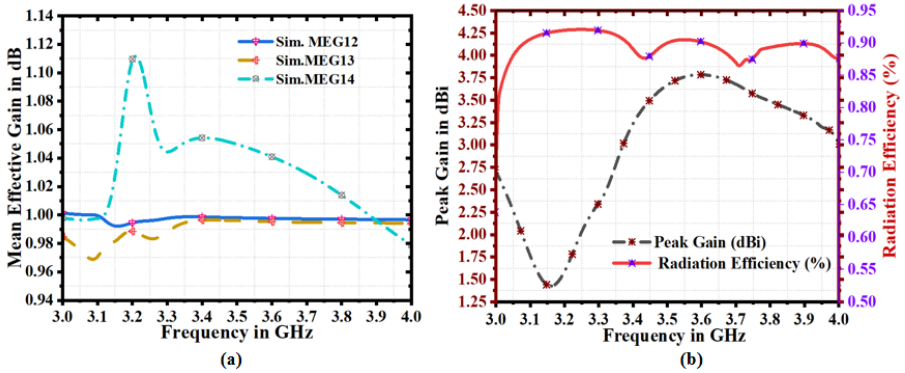

Fig. 11. Simulated results of the proposed 4-element MIMO antenna (a) MEG (dB) and (b) with and with out I-shaped decoupling-element(ISDE)

$$MEG_{i.} = 0.50[1-\Sigma_{j=1}^{N}|S_{ij}|^2] < -3dB,\ MEG_{j.} = 0.50[1-\Sigma_{i=1}^{N}|S_{ij}|^2 < -3dB \quad (7)$$

$$\left|\frac{MEG_{i.}}{MEG_{j.}}\right| = \pm 3dB\ or\ \left|MEG_{i.}-MEG_{j.}\right| = 3dB \quad (8)$$

S-parameters provide a simple method for calculating the MEG of two elements using Equations (7), and (8) [3, 5]. The simulated MEG results are presented in Fig. 11(a), showing a ratio between the two elements ranging from 0.98 to 1.12 dB.

Fig. 11(b) illustrates the simulated results for the peak gain and radiation efficiency of the proposed 4-element MIMO antenna. The peak gain reaches 3.9 dBi at 3.5 GHz, with an average peak gain of 3.34 dBi. The radiation efficiency ranges between 87% and 92%, as shown in Fig. 11(b).

Table 1: Comparative Analysis of Parameters from Literature Review and State-of-the-Art Research Compared to Existing Works

Ref. No, Year, No. of Ports	Antenna Size (mm^2)	space gap (mm)	impedance bandwidth (GHz)	Isolation Techniques $\|S_{21}\|$	Isolation (dB)	peak gain (dBi)	Radiation efficiency	ECC, DG(dB)	TARC (dB)	MEG (dB)	CCL (bits/s/Hz)
P.A 4	**$0.35\lambda_0$x$0.47\lambda_0$x$0.018\lambda_0$**	1.5	3.25-3.85	Stubs, protruded strip	19	3.259	92	0.011, 10	-10	0.481/1	0.3016
[33], 2024,4	**$0.54\lambda_0$x$0.54\lambda_0$**	8	3-4.12	Self isolation	21	4	84-96	0.005, 9.9	-5	-3	0.2
[17], 2023,4	**$0.80\lambda_0$x$0.80\lambda_0$**	N. R.	2.3-4.1 3.8-4.1 3.1-5.8	Symmetrical Folded branches	22	4.2	N.R.	0.021, 9.99	N.R.	N. R.	0.2
[27], 2022,4	**$1.2\lambda_0$x$0.87\lambda_0$**	N. R.	5.10-5.85	metallic	25	5	N.R.	0.004, 8	N.R.	N. R.	N.R.
[13], 2021,4	**$0.43\lambda_0$x$0.43\lambda_0$**	4.2	3.2-3.68 4.8-5.0	Parasitic Ground stub	16	4.4	N.R.	0.025, -	N.R.	N. R.	N.R.
[9], 2020,4	**$0.29\lambda_0$x$0.29\lambda_0$**	5	3.4-3.8	Mirrroring	18	5	N.R.	0.1, -	N.R.	N. R.	N.R.
[15], 2020,4	**$0.1.55\lambda_0$x$1.55\lambda_0$**	8	3.05-4.42	Stub	17	7-9.36	N.R.	N.R.	N.R.	N. R.	N.R.
[3], 2024,4	**$0.39\lambda_0\times1.51\lambda_0\times0.018\lambda_0$**	23	2.25-4.25	DGS, decoupling elements	21.5	4	90	0.12 / 9.9	-15	0.04	0.22
[33], 2024,4	**$0.75\lambda_0\times0.91\lambda_0\times0.018\lambda_0$**	16	2.21-2.25 2.55-3.65	DGS, decoupling elements	22.5	4.1	98	0.007 / 9.88	-10	0.048.	0.43

IV. CONCLUSION

This study presents a compact two-port MIMO antenna tailored for operation within the N78/48/77/79 bands, targeting 5G-NR FR-1 applications. Simulation results reveal enhanced performance and diversity for the proposed design. The SS-parameter characteristics (S_{xx} and S_{xy}) confirm effective coverage across the N78/48 band, with isolation (S_{21}) consistently exceeding -18.25 dB. Additionally, the paper explores the radiation pattern properties and MIMO diversity performance. The antenna is optimized for the N78/48 frequency range (3.15–3.89 GHz), making it suitable for 5G (FR-1 5G-NR), V2V, and V2D communication. Its versatility extends to non-wireless systems, including the ITU-T G.9963 home networking standard, as well as enterprise networks, fixed wireless access, and critical communication applications. Future work could aim to further reduce the antenna size and improve isolation by incorporating circular polarization and enhancing polarization diversity in the MIMO element design. Moreover, integrating machine learning techniques could broaden its applications in IoT, automation, biomedical fields, and emerging 6G technologies.

REFERENCES

[1] M. Agiwal, A. Roy, N. Saxena, Next generation 5g wireless networks: a com prehensive survey, IEEE communications surveys & tutorials 18 (3) (2016) 1617–1655.

[2] M. Fuentes, J.L. Carcel, C. Dietrich, L. Yu, E. Garro, V. Pauli, F.I. Lazarakis, O. Grøndalen, O. Bulakci, J. Yu, et al., 5g new radio evaluation against imt-2020 key performance indicators, IEEE Access 8 (2020) 110880–110896.

[3] Srinubabu, Manumula, and Nuthakki Venkata Rajasekhar. "Enhancing Diversity and Isolation Performance for a Four-Port Mimo Antenna in FR-1 5G Frequency Bands." IETE Journal of Research (2024): 1-16.

[4] T. Delson, I. Jose, A survey on 5g standards, specifications and massive mimo testbed including transceiver design models using qam modulation schemes, in: 2019 International Conference on Data Science and Communication (IconDSC), IEEE, 2019, pp. 1–7.

[5] S. Kumar, A.S. Dixit, R.R. Malekar, H.D. Raut, L.K. Shevada, Fifth genera tion antennas: a comprehensive review of design and performance enhancement techniques, IEEE Access 8 (2020) 163568–163593.

[6] M. Li, Y. Zhang, D. Wu, K.L. Yeung, L. Jiang, R. Murch, Decoupling and matching network for dual-band mimo antennas, IEEE Trans. Antenn. Propag. 70 (3) (2021) 1764–1775.

[7] M. Li, L. Jiang, K.L. Yeung, A novel wideband decoupling network for two antennas based on the wilkinson power divider, IEEE Trans. Antenn. Propag. 68 (7) (2020) 5082–5094.

[8] M. Alibakhshikenari, F. Babaeian, B.S. Virdee, S. A ¨ ıssa, L. Azpilicueta, C.H. See, A.A. Althuwayb, I. Huynen, R.A. Abd-Alhameed, F. Falcone, et al., A 20 comprehensive survey on "various decoupling mechanisms with focus on metama terial and metasurface principles applicable to sar and mimo antenna systems", IEEE Access 8 (2020) 192965–193004

[9] K.R. Jha, Z.P. Jibran, C. Singh, S.K. Sharma, 4-port mimo antenna using common radiator on a flexible substrate for sub-1ghz, sub-6ghz 5g nr, and wi f i 6 applications, IEEE Open Journal of Antennas and Propagation 2 (2021) 689–701.

[10] G. Saxena, P. Jain, Y.K. Awasthi, High diversity gain super-wideband single band-notch mimo antenna for multiple wireless applications, IET Microw., Antennas Propag. 14 (1) (2020) 109–119. Elabd, R.H.: Compact dual-port mimo filtenna-based dms with high isolation for c-band and x-band applications. EURASIP Journal on Wireless Communications and Networking 2023(1), 110 (2023).

[11] S. Zhang, G.F. Pedersen, Mutual coupling reduction for uwb mimo antennas with a wideband neutralization line, IEEE Antenn. Wireless Propag. Lett. 15 (2015) 166–169

[12] [T. Pan, Y. Sun, A dual-band compact four-element mimo antenna for sub 6g applications, in: 2021 International Conference on Microwave and Millimeter Wave Technology (ICMMT), IEEE, 2021, pp. 1–3.

[13] J. Kulkarni, R.K. Gangwar, J. Anguera, et al., Broadband and compact cir cularly polarized mimo antenna with concentric rings and oval slots for 5g application, IEEE Access 10 (2022) 29925–29936.

[14] J.-N. Sun, J.-L. Li, L. Xia, A dual-polarized magneto-electric dipole antenna for application to n77/n78 band, IEEE Access 7 (2019) 161708–161715.

[15] B. Nancharaiah, Basic compact two-element antenna with improved isolation using sub-6ghz for 5g applications, J. Data Acquis. Process. 38 (2) (2023) 3369.

[16] V. Saritha, C. Chandrasekhar, A conformal multi-band mimo antenna for vehic ular communications, Progress In Electromagnetics Research Letters 108 (2023) 49–57.

[17] S.R. Patre, S.P. Singh, Broadband multiple-input–multiple-output antenna using castor leaf-shaped quasi-self-complementary elements, IET Microw., Antennas Propag. 10 (15) (2016) 1673–1681.

[18] Z. Wang, Y. Ning, Y. Dong, Compact shared aperture quasi-yagi antenna with pattern diversity for 5g-nr applications, IEEE Trans. Antenn. Propag. 69 (7) (2020) 4178–4183, 21.

[19] Y. Qin, L. Zhang, C.-X. Mao, H. Zhu, A compact wideband antenna with sup pressed mutual coupling for 5g mimo applications, IEEE Antenn. Wireless Propag. Lett. 22 (4) (2022) 938–942.

[20] S. Kumar, S.K. Palaniswamy, H.C. Choi, K.W. Kim, Compact dual circularly polarized quad-element mimo/diversity antenna for sub-6 ghz communication systems, Sensors 22 (24) (2022) 9827.

[21] M. Alibakhshikenari, B.S. Virdee, C.H. See, R.A. Abd-Alhameed, F. Falcone, E. Limiti, Surface wave reduction in antenna arrays using metasurface inclusion for mimo and sar systems, Radio Sci. 54 (11) (2019) 1067–1075.

[22] H. Sudarsan, R. Gayathri, K. Mahendran, A novel square fractal dual port mimo antenna with tri band rejection capabilities, J. Ambient Intell. Hum. Comput. (2021) 1–18.

[23] N. Kumar, K.U. Kiran, Meander-line electromagnetic bandgap structure for uwb mimo antenna mutual coupling reduction in e-plane, AEU-International Journal of Electronics and Communications 127 (2020) 153423.

[24] L. Min, J. Yasir, K. Yeung, et al., A novel dual-band decoupling technique [j], IEEE Trans. Antenn. Propag. 68 (10) (2020) 6923–6934.

[25] S.K. Mahto, A.K. Singh, R. Sinha, M. Alibakhshikenari, S. Khan, G. Pau, High isolated four element mimo antenna for ism/lte/5g (sub-6ghz) applications, IEEE Access (2023).

[26] S.K. Mahto, A.K. Singh, R. Sinha, M. Alibakhshikenari, S. Khan, G. Pau, High isolated four element mimo antenna for ism/lte/5g (sub-6ghz) applications, IEEE Access (2023).

[27] A. Pant, M. Singh, M.S. Parihar, A frequency reconfigurable/switchable mimo antenna for lte and early 5g applications, AEU-international Journal of Electronics and Communications 131 (2021) 153638.

[28] M.A. Abdelghany, A.A. Ibrahim, H.A. Mohamed, E. Tammam, Compact sub 6 ghz four-element flexible antenna for 5g applications, Electronics 13 (3) (2024) 537

[29] T. Islam, E.M. Ali, W.A. Awan, M.S. Alzaidi, T.A. Alghamdi, M. Alathbah, A parasitic patch loaded staircase shaped uwb mimo antenna having notch band for wban applications, Heliyon 10 (1) (2024)

[30] E. Saenz, K. Guven, E. Ozbay, I. Ederra, R. Gonzalo, et al., Decoupling of multifrequency dipole antenna arrays for microwave imaging applications, Int. J. Antenn. Propag. 2010 (2010)

[31] Twopence-fed MIMO Antenna with Wide Bandwidth and High Isolation for Future Wireless Applications.

[32] Manumula, Srinubabu, and N. V. Rajasekhar. "Design of compact MIMO antenna for 5G Applications." 2023 3rd International conference on Artificial Intelligence and Signal Processing (AISP). IEEE, 2023.

[33] Srinubabu, Manumula, and Nuthakki Venkata Rajasekhar. "Design and Analysis of a Compact 4-Port MIMO Antenna for Improved Isolation and 5G (n78/n77/n48) Performance." Traitement du Signal 41.4 (2024): 2057.